Supplementary Material

A theoretical model on the formation mechanism and kinetics of highly toxic air pollutants from halogenated formaldehydes reacted with halogen atoms

Y.M. Ji[1], H.H. Wang[1,2], Y.P. Gao[1,2], G.Y. Li [1], and T.C. An[1,*]

[1] State Key Laboratory of Organic Geochemistry and Guangdong Key Laboratory of Environmental Resources Utilization and Protection, Guangzhou Institute of Geochemistry, Chinese Academy of Sciences, Guangzhou 510640, China;

[2] Graduate School of Chinese Academy of Sciences, Beijing 100049, China.

Correspondence to: T.C. An (antc99@gig.ac.cn)

■ RESULTS AND DISCUSSION

Rate Constants. The canonical variational transition state theory (CVT) (Truhlar et al., 1980) rate constant can be obtained by variationally minimizing the generalized transition-state theory rate constant $k^{GT}(T,s)$ with respect to the dividing surface at s, that is,

$$k^{CVT}(T) = \min_{s} k^{GT}(T,s) \quad (1)$$

where

$$k^{GT}(T,s) = \frac{\sigma}{h\beta}\frac{Q^{GT}(T,s)}{Q^{R}(T)}\exp[-\beta V_{MEP}(s)] \quad (2)$$

In these equations, s is the location of the generalized transition state on the intrinsic reaction coordinate (IRC); σ is the symmetry factor accounting for the possibility of two or more symmetry-related reaction paths; β equals $(k_B T)^{-1}$ where k_B is Boltzmann's constant, h is Planck's constant; $Q^R(T)$ is the reactant's partition function per unit volume, excluding symmetry numbers for rotation; $V_{MEP}(s)$ is the classical energy along the minimum-energy path (MEP) overall zero of energy at the reactants; $Q^{GT}(T,s)$ is the partition function of

generalized transition state at s with the local zero of energy at $V_{MEP}(s)$ and with all rotational symmetry numbers set to unity. To include the tunneling effect, the CVT rate constant is multiplied by a transmission coefficient computed with the small-curvature tunneling (SCT) (Liu et al., 1993) approximation, which is denoted by k(CVT/SCT). The total rate constants for the title reactions are obtained from the sum of the individual rate constants associated.

Branching Ratio. The branching ratio Γ of each pathways was determined on the following equation, $\Gamma_n = \frac{k_n}{\sum_n k_n}$, where k_n is the reaction rate constants of nth pathway. In this work, the total CVT/SCT rate constants for each atmospheric reaction were obtained as the sum of the individual rate constants associated with the H-abstraction and X-addition pathways.

The Atmospheric Fate of ClCO Radical. To confirm the no barrier of these processes, the point-wise potential curve was calculated and the results is shown in Figure S7-S9. For the pathways 2 and 3, the forming C–O bonds were fixed at the values from 1.1 to 2.7 Å and from 1.2 to 3.2 Å with the interval of 0.1 Å, respectively, and the other geometric parameters were optimized for each C–O value. The minimum energy in these two pathways appeared at the C–O distance of 1.4 Å, leading to intermediates *tran*-$ClCO_3$ and *cis*-$ClCO_3$, respectively. As for the pathway 4, the forming C–Cl bond was fixed at the values from 1.3 to 4.5 Å with the interval of 0.1Å, and the other geometric parameters were optimized for each C–Cl value. The minimum energy appeared at the C–Cl distance of 1.8 Å, leading to phosgene.

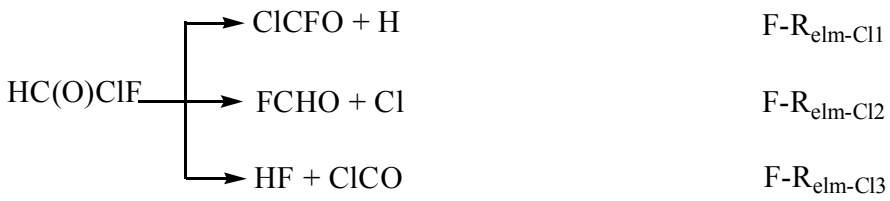

Scheme S1. For the addition intermediate HC(O)ClF, three degradation pathways: H-elimination, Cl-elimination, and HF-elimination pathways

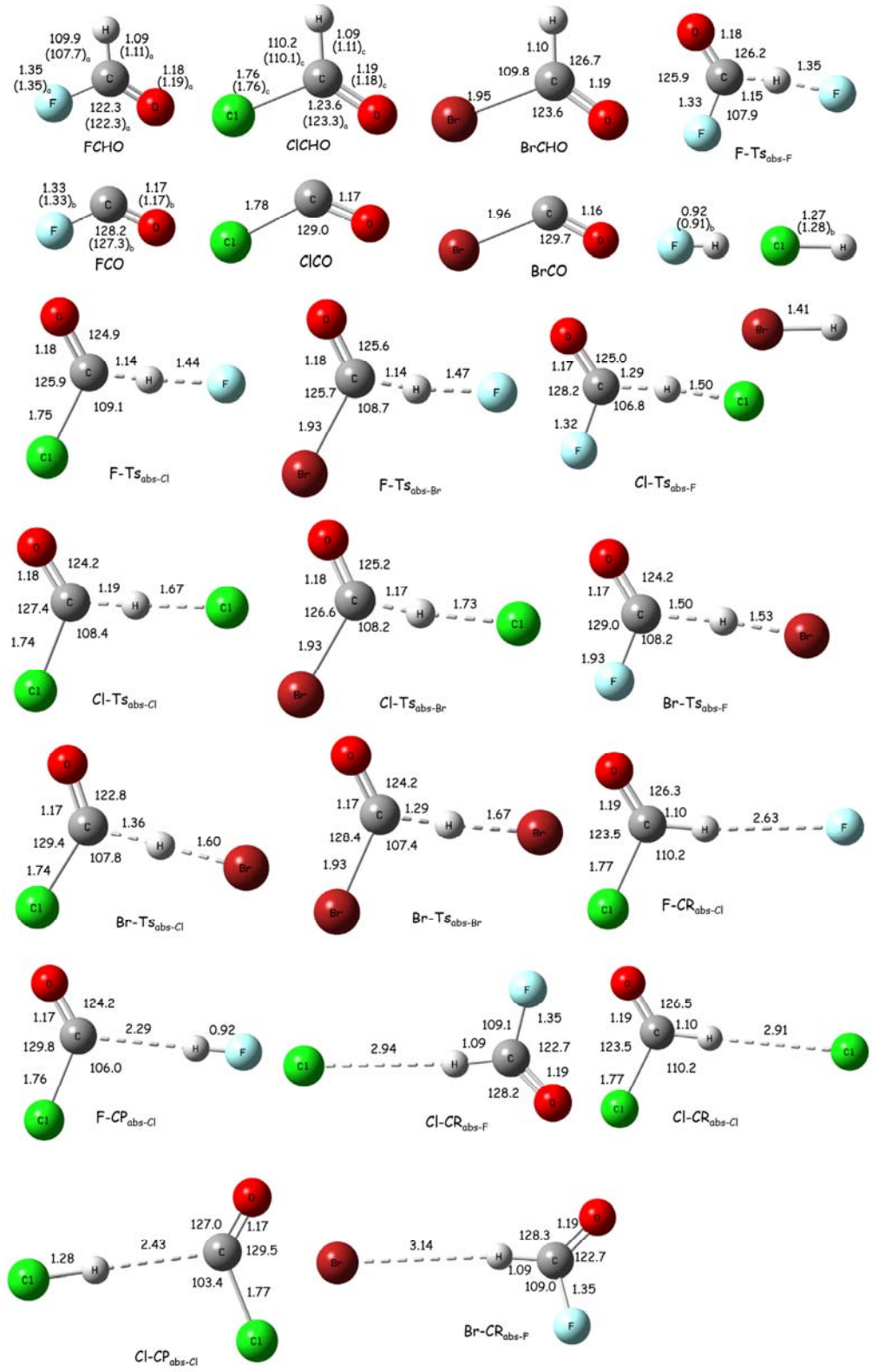

Fig. S1. Optimized geometries of reactants, transition states, complexes, and products involved in the H-abstraction pathways at the PMP2/6-311+G(d,p) level as well as the available experimental data. (Groner et al., 2001; Huisman et al., 1979; Nagai et al., 1981; NIST). (Bond lengths are in Å and angles are in °.)

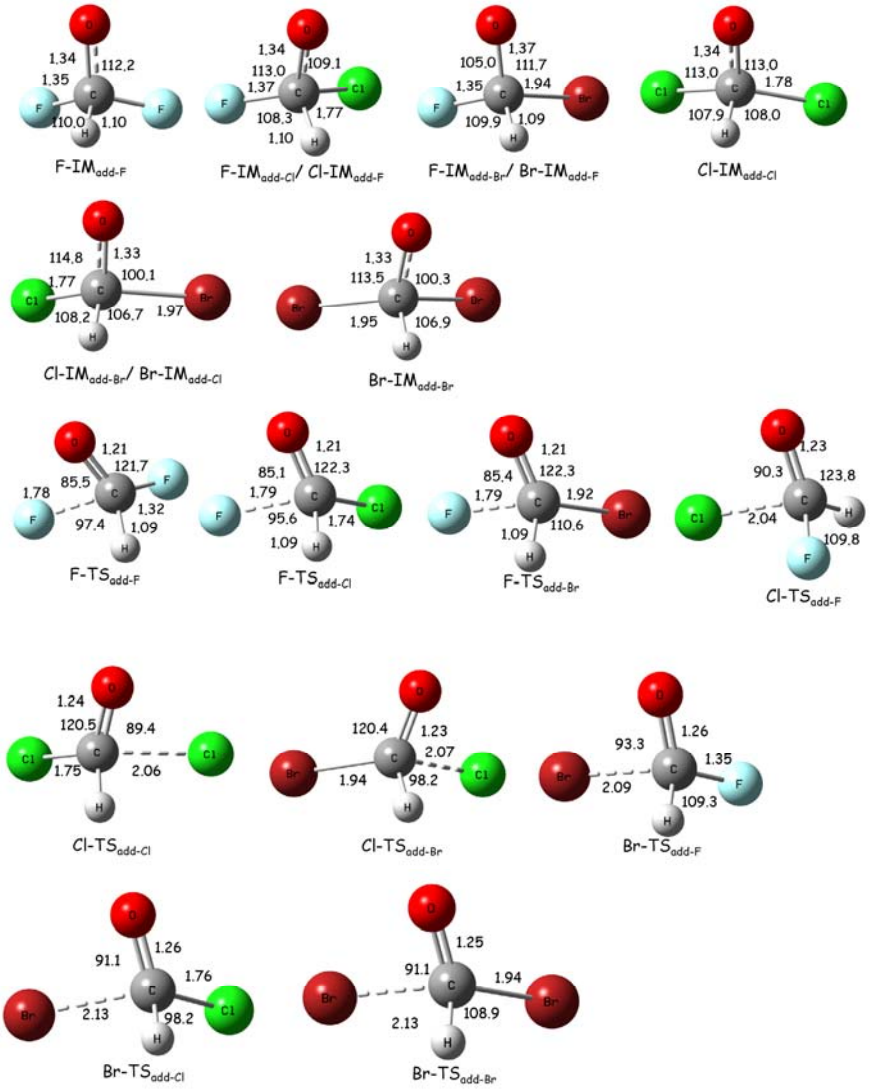

Fig. S2. Optimized geometries of reactants, transition states, intermediates and products involved in the X-addition pathways at the PMP2/6-311+G(d,p) level. (Bond lengths are in Å and angles are in °.)

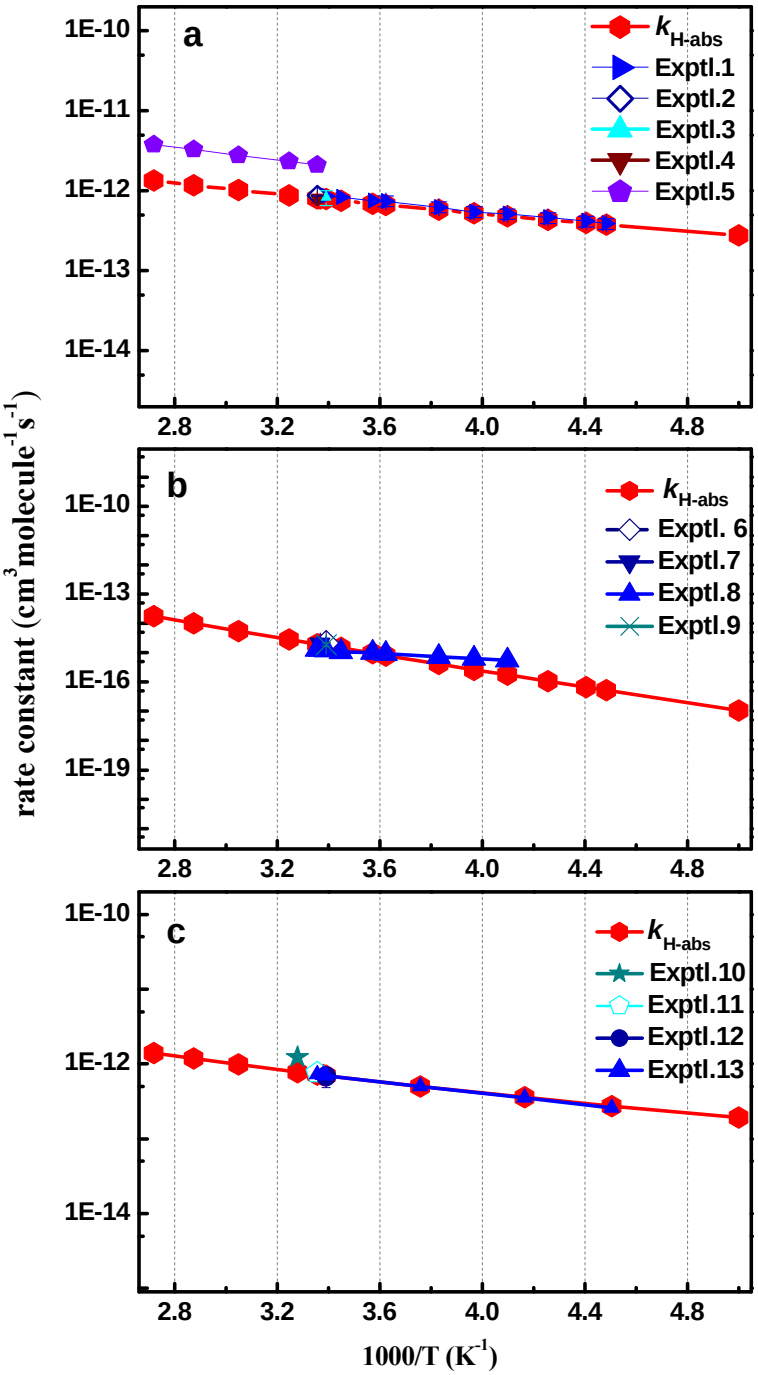

Fig. S3. Plot of the CVT/SCT rate constants calculated at the QCISD(T)//PMP2 level and the available experimental values vs 1000/T between 200–368 K for the H-abstraction pathways of (a) FCHO with F, (b) FCHO with Cl, and (c) ClCHO with Cl. Exptl. 1 from (Behr et al., 1998); Exptl. 2 from (Behr et al., 1993); Exptl. 3 from (Meagher et al., 1997); Exptl. 4 from (Hasson et al., 1998); Exptl. 5 from (Francisco et al., 1990); Exptl. 6 from (Edney et al., 1992); Exptl. 7 from (Wallington et al., 1992); Exptl. 8 from (Bednarek et al., 1996); Exptl. 9 from (Meagher et al., 1997); Exptl. 10 from (Sanhueza et al., 1975); Exptl. 11 from (Libuda et al., 1990); Exptl. 12 from (Wallington et al., 1996); Exptl. 13 from (Orlando, 1999); Exptl. 14 from (Catoire et al., 1996).

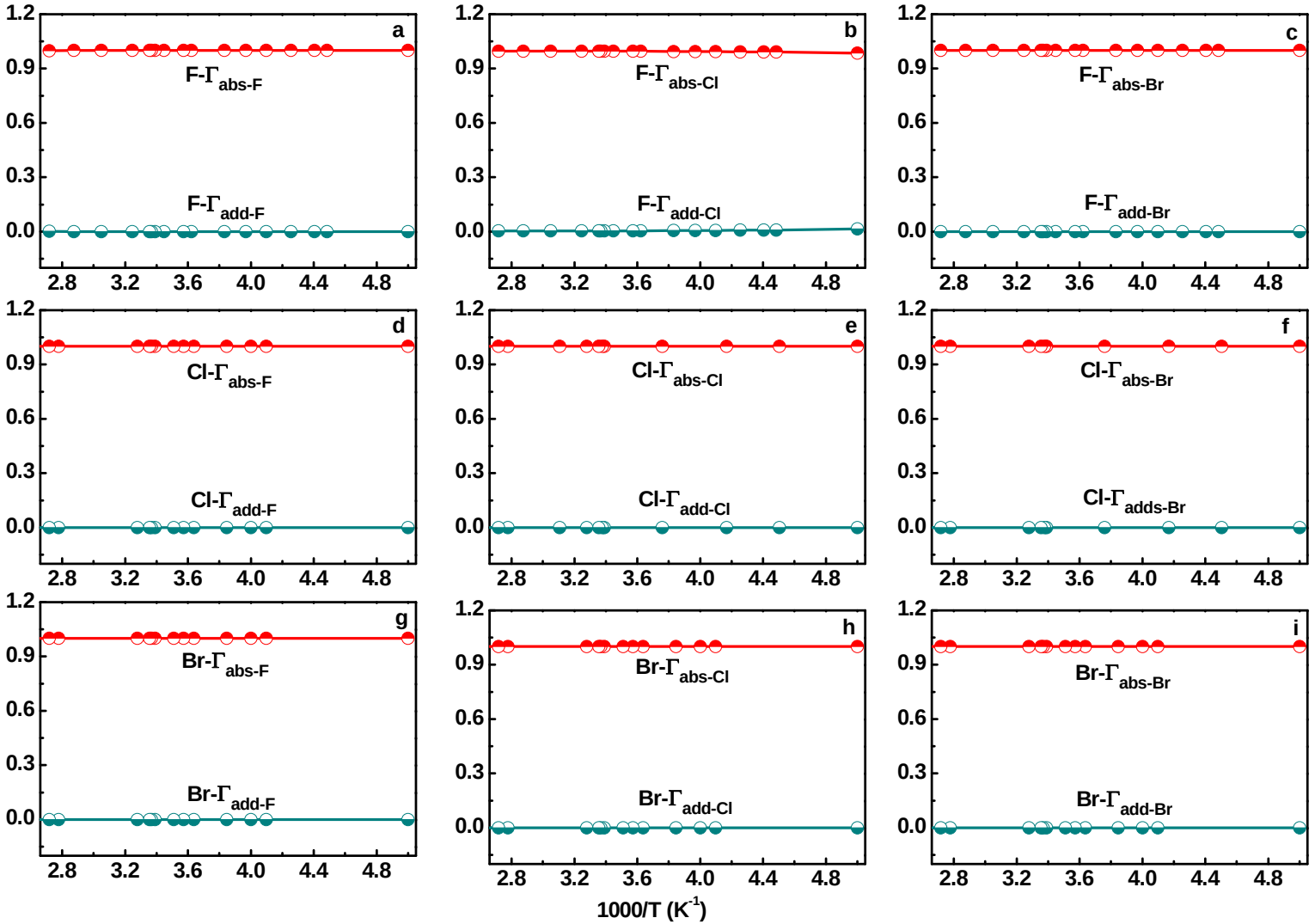

Fig. S4. Plot of calculated branching ratio of the H-abstraction and X-addition pathways versus 1000/*T* between 200 and 368 K for the reactions of (a) FCHO with F, (b) ClCHO with F, (c) BrCHO with F, (d) FCHO with Cl, (e) ClCHO with Cl, (f) BrCHO with Cl, (g) FCHO with Br, (h) ClCHO with Br and (i) BrCHO with Br.

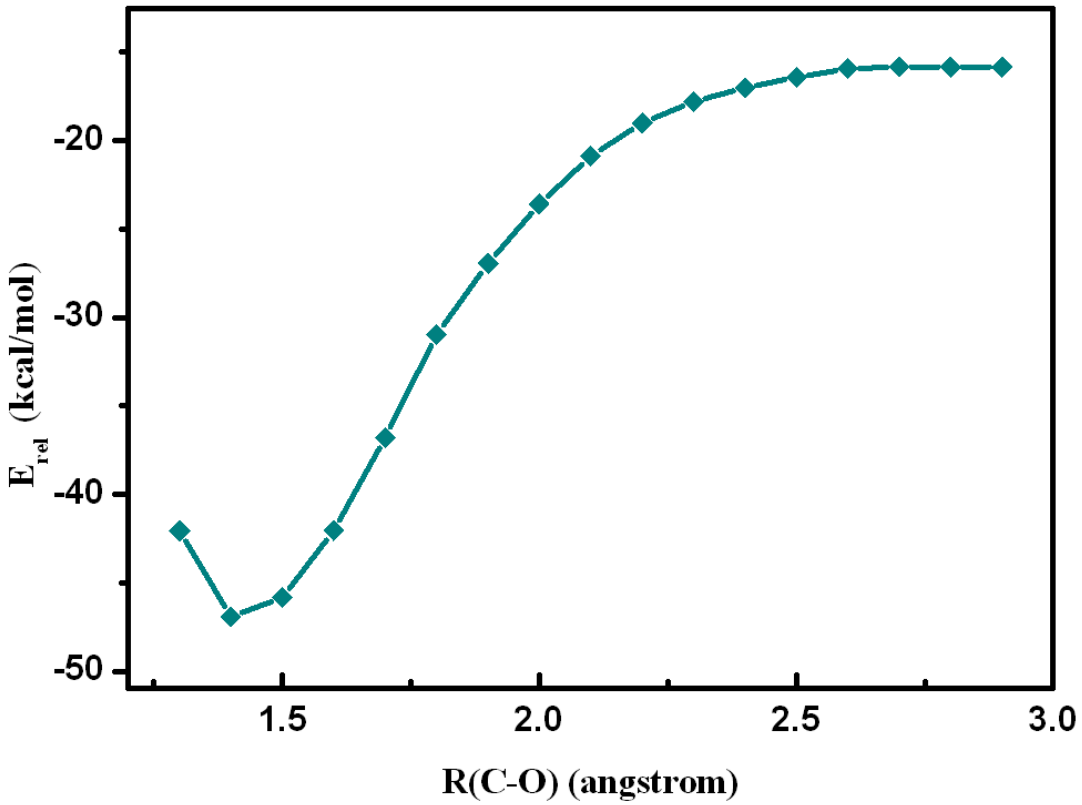

Fig. S5. Potential energy curve for the formative process of *trans*-$CClO_3$ at the PMP2/6-311+G(d,p) level. The dotted line denotes the relative energy of $ClCO + O_2$.

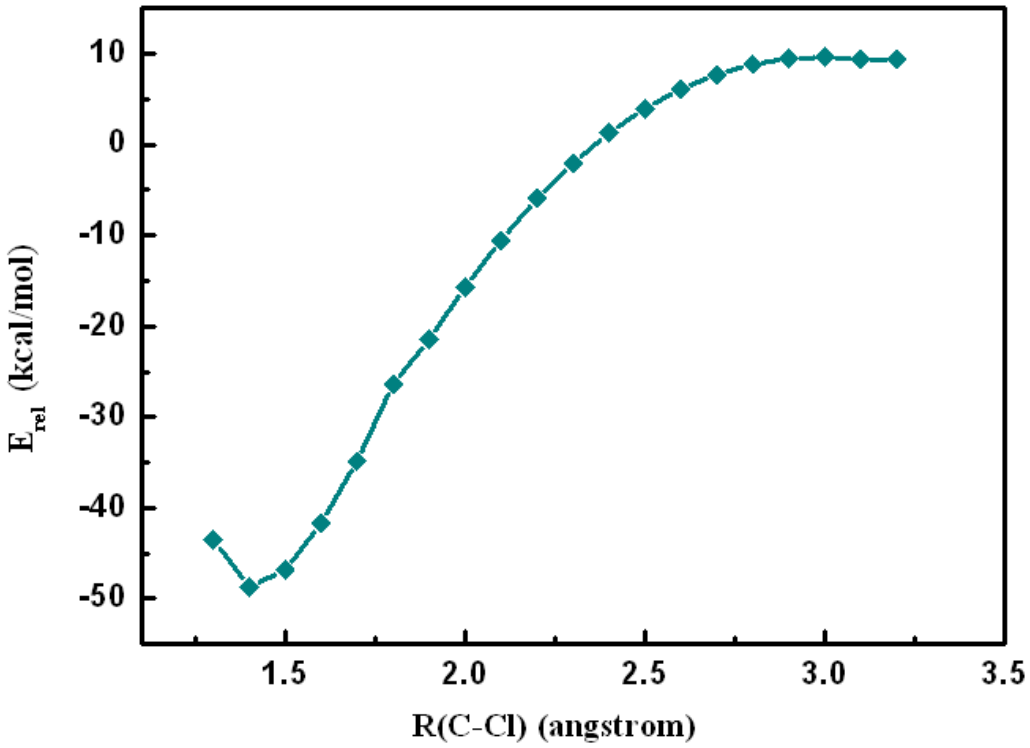

Fig. S6. Potential energy curve for the formative process of *cis*-$CClO_3$ at the PMP2/6-311+G(d,p) level. The dotted line denotes the relative energy of $ClCO + O_2$.

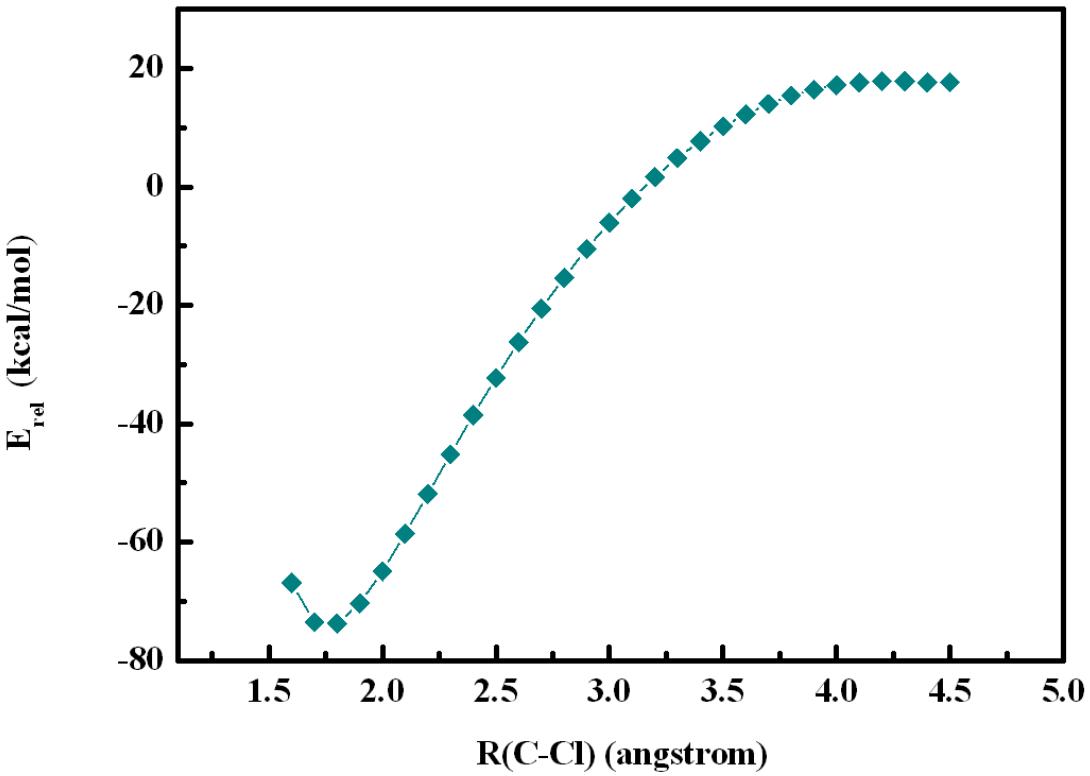

Fig. S7. Potential energy curve for the formative process of phosgene at the PMP2/6-311+G(d,p) level. The dotted line denotes the relative energy of ClCO + Cl.

Table S1. Calculated frequencies of the stationary points at the PMP2/6-311+G(d,p) level. (unit: cm^{-1})

species	ν	species	ν
FCHO	662, 1042, 1061, 1396, 1860, 3167	ClCHO	473, 769, 970, 1386, 1795, 3109
BrCHO	369, 661, 926, 1344, 1795, 3097	FCO	636, 1053, 1989
ClCO	396, 648, 1961	BrCO	289, 563, 1934
HF	4199	HCl	3087
HBr	2739	$F\text{-}IM_{add\text{-}F}$	471, 517, 651, 1003, 1122, 1158, 1335, 1399, 3095
$F\text{-}IM_{add\text{-}Cl}$/$Cl\text{-}IM_{add\text{-}F}$	248, 405, 584, 771, 1033, 1098, 1242, 1335, 3101	$F\text{-}IM_{add\text{-}Br}$/$Br\text{-}IM_{add\text{-}F}$	318, 354, 532, 722, 1089, 1151, 1344, 1429, 3167
$Cl\text{-}IM_{add\text{-}Cl}$	296, 334, 450, 698, 808, 1067, 1214, 1257, 3057	$Cl\text{-}IM_{add\text{-}Br}$/$Br\text{-}IM_{add\text{-}Cl}$	217, 311, 59, 603, 1017, 1134, 1153, 1364, 3139
$Br\text{-}IM_{add\text{-}Br}$	160, 276, 329, 564, 659, 1084, 1151, 1273, 3141	$F\text{-}TS_{abs\text{-}F}$	1445*i*, 85, 139, 621, 856, 986, 1098, 1335, 1952
$F\text{-}TS_{abs\text{-}Cl}$	761*i*, 77, 157, 470, 751, 952, 1261, 1413, 1931	$F\text{-}TS_{abs\text{-}Br}$	636*i*, 65, 142, 371, 611, 903, 1223, 1606, 1916
$Cl\text{-}TS_{abs\text{-}F}$	1615*i*, 109, 207, 327, 699, 917, 1089, 1122, 2025	$Cl\text{-}TS_{abs\text{-}Cl}$	1005*i*, 81, 189, 435, 576, 811, 937, 1238, 2008
$Cl\text{-}TS_{abs\text{-}Br}$	594*i*, 64, 167, 371, 567, 899, 992, 1252, 1967	$Br\text{-}TS_{abs\text{-}F}$	815*i*, 95, 179, 406, 735, 736, 888, 1097, 2016
$Br\text{-}TS_{abs\text{-}Cl}$	1175*i*, 88, 215, 253, 509, 761, 848, 1039, 2040	$Br\text{-}TS_{abs\text{-}Br}$	1321*i*, 68, 203, 230, 380, 683, 851, 1091, 2018
$F\text{-}TS_{add\text{-}F}$	1215*i*, 298, 418, 682, 1070, 1141, 1408, 1614, 3201	$F\text{-}TS_{add\text{-}Cl}$	1192*i*, 245, 397, 491, 812, 1038, 1398, 1551, 3157
$F\text{-}TS_{add\text{-}Br}$	1206*i*, 209, 364, 415, 695, 1025, 1360, 1543, 3140	$Cl\text{-}TS_{add\text{-}F}$	914*i*, 278, 357, 650, 959, 1116, 1360, 1449, 3173
$Cl\text{-}TS_{add\text{-}Cl}$	888*i*, 222, 339, 468, 770, 969, 1359, 1388, 3143	$Cl\text{-}TS_{add\text{-}Br}$	892*i*, 179, 330, 372, 660, 962, 1322, 1378, 3129
$Br\text{-}TS_{add\text{-}F}$	632*i*, 271, 302, 628, 905, 1102, 1312, 1400, 3156	$Br\text{-}TS_{add\text{-}Cl}$	632, 271, 302, 628, 905, 1102, 1312, 1400, 3156
$Br\text{-}TS_{add\text{-}Br}$	703*i*, 150, 289, 359, 641, 926, 1304, 1318, 3124		
$F\text{-}CP_{F}$	36, 38, 121, 384, 386, 656, 1101, 1941, 4124	$F\text{-}CR_{Cl}$	13, 51, 69, 473, 766, 983, 1392, 1792, 3134
$F\text{-}CP_{Cl}$	33, 74, 126, 361, 396, 426, 677, 1905, 4107	$F\text{-}CR_{Br}$	24, 43, 52, 365, 656, 928, 1338, 1801, 3111
$Cl\text{-}CR_{F}$	20, 54, 71, 662, 1058, 1058, 1403, 1858, 3185	$Cl\text{-}CR_{Cl}$	5, 54, 72, 471, 762, 987, 1395, 1794, 3133
$Cl\text{-}CP_{Cl}$	22, 56, 80, 226, 260, 412, 662, 1930, 3030	$Cl\text{-}CR_{Br}$	30, 46, 59, 359, 647, 927, 1332, 1808, 3112
$Br\text{-}CR_{F}$	20, 39, 62, 661, 1055, 1056, 1401, 1857, 3177	$Br\text{-}CP_{Cl}$	19, 44, 65, 195, 222, 409, 659, 1936, 2687

Table S2. The imaginary frequencies and parameter L at the PMP2 level. (ν in cm^{-1})

	F		Cl		Br	
	ν	L	ν	L	ν	L
FCHO	1445*i*	0.14	1615*i*	0.87	815*i*	1.05
ClCHO	761*i*	0.10	1005*i*	0.25	1175*i*	1.42
BrCHO	636*i*	0.07	594*i*	0.15	1321*i*	0.73

Table S3. The relative energies of complexes. (in kcal/mol)	
Complex	ΔE
F-$CR_{abs\text{-}Cl}$	−0.47
F-$CP_{abs\text{-}Cl}$	−43.94
Cl-$CR_{abs\text{-}Cl}$	−2.41
Cl-$CP_{abs\text{-}Cl}$	−11.05
Cl-$CR_{abs\text{-}F}$	−0.66
Br-$CR_{abs\text{-}F}$	−0.69

Table S4. The enthalpies of formation ($\Delta H^{0}_{f,298}$) of the main species at QCISD(T)//PMP2 level. (in kcal/mol)

species	enthalpies	species	enthalpies
FCHO	–92.6 [a](–89.96)	FCO	–41.5 [a](–41.04)
ClCHO	–46.2	ClCO	–5.1
BrCHO	–32.8	BrCO	3.4

[a] Expeimental values.(NIST)

Table S5. Calculated CVT/SCT rate constants of H-abstraction and X-addition pathways of the F + QCHO reaction system. (in cm^3 $molecule^{-1}$ s^{-1})

T(*K*)	F + FCHO → products			F + ClCHO → products			F + BrCHO → products		
	F-$k_{abs\text{-}F}$	F-$k_{add\text{-}F}$	k_{total}	F-$k_{abs\text{-}Cl}$	F-$k_{add\text{-}Cl}$	k_{total}	F-$k_{abs\text{-}Br}$	F-$k_{add\text{-}Br}$	k_{total}
200	2.77×10^{-13}	4.14×10^{-19}	2.77×10^{-13}	2.57×10^{-12}	4.66×10^{-20}	2.57×10^{-12}	4.95×10^{-12}	7.07×10^{-21}	4.95×10^{-12}
223	3.76×10^{-13}	2.12×10^{-18}	3.76×10^{-13}	2.94×10^{-12}	2.32×10^{-19}	2.94×10^{-12}	5.69×10^{-12}	1.08×10^{-20}	5.69×10^{-12}
227	3.95×10^{-13}	2.75×10^{-18}	3.95×10^{-13}	3.00×10^{-12}	3.06×10^{-19}	3.00×10^{-12}	5.83×10^{-12}	1.17×10^{-20}	5.83×10^{-12}
235	4.35×10^{-13}	4.51×10^{-18}	4.35×10^{-13}	3.13×10^{-12}	5.26×10^{-19}	3.13×10^{-12}	6.09×10^{-12}	1.39×10^{-20}	6.09×10^{-12}
244	4.81×10^{-13}	7.65×10^{-18}	4.81×10^{-13}	3.28×10^{-12}	9.44×10^{-19}	3.28×10^{-12}	6.39×10^{-12}	1.72×10^{-20}	6.39×10^{-12}
252	5.25×10^{-13}	1.19×10^{-17}	5.25×10^{-13}	3.42×10^{-12}	1.55×10^{-18}	3.42×10^{-12}	6.67×10^{-12}	2.14×10^{-20}	6.67×10^{-12}
261	5.76×10^{-13}	1.90×10^{-17}	5.76×10^{-13}	3.57×10^{-12}	2.63×10^{-18}	3.57×10^{-12}	6.98×10^{-12}	2.82×10^{-20}	6.98×10^{-12}
276	6.66×10^{-13}	3.92×10^{-17}	6.66×10^{-13}	3.83×10^{-12}	5.99×10^{-18}	3.83×10^{-12}	7.50×10^{-12}	4.81×10^{-20}	7.50×10^{-12}
280	6.91×10^{-13}	4.70×10^{-17}	6.91×10^{-13}	3.91×10^{-12}	7.37×10^{-18}	3.91×10^{-12}	7.64×10^{-12}	5.63×10^{-20}	7.64×10^{-12}
290	7.55×10^{-13}	7.26×10^{-17}	7.55×10^{-13}	4.08×10^{-12}	1.21×10^{-17}	4.08×10^{-12}	7.99×10^{-12}	8.44×10^{-20}	7.99×10^{-12}
295	7.88×10^{-13}	8.93×10^{-17}	7.88×10^{-13}	4.17×10^{-12}	1.54×10^{-17}	4.17×10^{-12}	8.17×10^{-12}	1.04×10^{-19}	8.17×10^{-12}
297	8.02×10^{-13}	9.68×10^{-17}	8.02×10^{-13}	4.21×10^{-12}	1.68×10^{-17}	4.21×10^{-12}	8.24×10^{-12}	1.13×10^{-19}	8.24×10^{-12}
298	8.08×10^{-13}	1.01×10^{-16}	8.08×10^{-13}	4.23×10^{-12}	1.76×10^{-17}	4.23×10^{-12}	8.28×10^{-12}	1.18×10^{-19}	8.28×10^{-12}
308	8.77×10^{-13}	1.49×10^{-16}	8.77×10^{-13}	4.41×10^{-12}	2.76×10^{-17}	4.41×10^{-12}	8.64×10^{-12}	1.80×10^{-19}	8.64×10^{-12}
328	1.02×10^{-12}	3.04×10^{-16}	1.02×10^{-12}	4.78×10^{-12}	6.26×10^{-17}	4.78×10^{-12}	9.37×10^{-12}	4.16×10^{-19}	9.37×10^{-12}
348	1.18×10^{-12}	5.76×10^{-16}	1.18×10^{-12}	5.16×10^{-12}	1.31×10^{-16}	5.16×10^{-12}	1.01×10^{-11}	9.15×10^{-19}	1.01×10^{-11}
368	1.34×10^{-12}	1.03×10^{-15}	1.34×10^{-12}	5.55×10^{-12}	2.54×10^{-16}	5.55×10^{-12}	1.09×10^{-11}	1.90×10^{-18}	1.09×10^{-11}

Table S6. Calculated CVT/SCT rate constants of H-abstraction and X-addition pathways of the Cl + QCHO reaction system. (in cm^3 $molecule^{-1}$ s^{-1})

T(*K*)	Cl + FCHO → products			Cl + ClCHO → products			Cl + BrCHO → products		
	Cl-$k_{abs\text{-}F}$	Cl-$k_{add\text{-}F}$	k_{total}	Cl-$k_{abs\text{-}Cl}$	Cl-$k_{add\text{-}Cl}$	k_{total}	Cl-$k_{abs\text{-}Br}$	Cl-$k_{add\text{-}Br}$	k_{total}
200	1.08×10^{-17}	5.81×10^{-30}	1.08×10^{-17}	1.94×10^{-13}	3.25×10^{-38}	1.94×10^{-13}	6.41×10^{-13}	2.09×10^{-28}	6.41×10^{-13}
223	5.23×10^{-17}	2.25×10^{-28}	5.23×10^{-17}	2.79×10^{-13}	4.28×10^{-36}	2.79×10^{-13}	7.69×10^{-13}	8.19×10^{-27}	7.69×10^{-13}
227	6.69×10^{-17}	3.96×10^{-28}	6.69×10^{-17}	2.96×10^{-13}	9.06×10^{-36}	2.96×10^{-13}	7.93×10^{-13}	1.44×10^{-26}	7.93×10^{-13}
235	1.07×10^{-16}	1.16×10^{-27}	1.07×10^{-16}	3.33×10^{-13}	3.76×10^{-35}	3.33×10^{-13}	8.42×10^{-13}	4.21×10^{-26}	8.42×10^{-13}
244	1.75×10^{-16}	3.63×10^{-27}	1.75×10^{-16}	3.77×10^{-13}	1.67×10^{-34}	3.77×10^{-13}	9.00×10^{-13}	1.29×10^{-25}	9.00×10^{-13}
252	2.65×10^{-16}	9.37×10^{-27}	2.65×10^{-16}	4.20×10^{-13}	5.78×10^{-34}	4.20×10^{-13}	9.54×10^{-13}	3.30×10^{-25}	9.54×10^{-13}
261	4.11×10^{-16}	2.56×10^{-26}	4.11×10^{-16}	4.71×10^{-13}	2.13×10^{-33}	4.71×10^{-13}	1.02×10^{-12}	8.80×10^{-25}	1.02×10^{-12}
276	8.08×10^{-16}	1.19×10^{-25}	8.08×10^{-16}	5.66×10^{-13}	1.56×10^{-32}	5.66×10^{-13}	1.13×10^{-12}	3.95×10^{-24}	1.13×10^{-12}
280	9.57×10^{-16}	1.75×10^{-25}	9.57×10^{-16}	5.93×10^{-13}	2.57×10^{-32}	5.93×10^{-13}	1.16×10^{-12}	5.75×10^{-24}	1.16×10^{-12}
290	1.44×10^{-15}	4.40×10^{-25}	1.44×10^{-15}	6.65×10^{-13}	8.37×10^{-32}	6.65×10^{-13}	1.24×10^{-12}	1.40×10^{-23}	1.24×10^{-12}
295	1.74×10^{-15}	6.83×10^{-25}	1.74×10^{-15}	7.02×10^{-13}	1.47×10^{-31}	7.02×10^{-13}	1.28×10^{-12}	2.14×10^{-23}	1.28×10^{-12}
297	1.88×10^{-15}	8.11×10^{-25}	1.88×10^{-15}	7.18×10^{-13}	1.83×10^{-31}	7.18×10^{-13}	1.30×10^{-12}	2.53×10^{-23}	1.30×10^{-12}
298	1.95×10^{-15}	8.83×10^{-25}	1.95×10^{-15}	7.25×10^{-13}	2.04×10^{-31}	7.25×10^{-13}	1.31×10^{-12}	2.74×10^{-23}	1.31×10^{-12}
308	2.81×10^{-15}	2.01×10^{-24}	2.81×10^{-15}	8.06×10^{-13}	5.83×10^{-31}	8.06×10^{-13}	1.39×10^{-12}	6.05×10^{-23}	1.39×10^{-12}
328	5.50×10^{-15}	9.11×10^{-24}	5.50×10^{-15}	9.84×10^{-13}	3.96×10^{-30}	9.84×10^{-13}	1.58×10^{-12}	2.56×10^{-22}	1.58×10^{-12}
348	1.01×10^{-14}	3.51×10^{-23}	1.01×10^{-14}	1.18×10^{-12}	2.18×10^{-29}	1.18×10^{-12}	1.77×10^{-12}	9.23×10^{-22}	1.77×10^{-12}
368	1.74×10^{-14}	1.19×10^{-22}	1.74×10^{-14}	1.41×10^{-12}	1.00×10^{-28}	1.41×10^{-12}	1.99×10^{-12}	2.91×10^{-21}	1.99×10^{-12}

Table S7. Calculated CVT/SCT rate constants of H-abstraction and X-addition pathways of the Br + QCHO reaction system. (in cm^3 $molecule^{-1}$ s^{-1})

T(*K*)	Br + FCHO → products			Br + ClCHO → products			Br + BrCHO → products		
	Br-$k_{abs\text{-}F}$	Br-$k_{add\text{-}F}$	k_{total}	Br-$k_{abs\text{-}Cl}$	Br-$k_{add\text{-}Cl}$	k_{total}	Br-$k_{abs\text{-}Br}$	Br-$k_{add\text{-}Br}$	k_{total}
200	2.48×10^{-27}	5.28×10^{-42}	2.48×10^{-27}	1.36×10^{-17}	3.45×10^{-40}	1.36×10^{-17}	5.97×10^{-16}	6.06×10^{-36}	5.97×10^{-16}
223	1.43×10^{-25}	9.01×10^{-39}	1.43×10^{-25}	6.03×10^{-17}	2.98×10^{-37}	6.03×10^{-17}	1.42×10^{-15}	1.22×10^{-33}	1.42×10^{-15}
227	2.67×10^{-25}	2.82×10^{-38}	2.67×10^{-25}	7.59×10^{-17}	8.40×10^{-37}	7.59×10^{-17}	1.63×10^{-15}	2.75×10^{-33}	1.63×10^{-15}
235	8.82×10^{-25}	2.47×10^{-37}	8.82×10^{-25}	1.18×10^{-16}	6.02×10^{-36}	1.18×10^{-16}	2.12×10^{-15}	1.29×10^{-32}	2.12×10^{-15}
244	3.09×10^{-24}	2.39×10^{-36}	3.09×10^{-24}	1.88×10^{-16}	4.74×10^{-35}	1.88×10^{-16}	2.80×10^{-15}	6.52×10^{-32}	2.80×10^{-15}
252	8.79×10^{-24}	1.58×10^{-35}	8.79×10^{-24}	2.77×10^{-16}	2.63×10^{-34}	2.77×10^{-16}	3.53×10^{-15}	2.50×10^{-31}	3.53×10^{-15}
261	2.65×10^{-23}	1.15×10^{-34}	2.65×10^{-23}	4.17×10^{-16}	1.59×10^{-33}	4.17×10^{-16}	4.52×10^{-15}	1.03×10^{-30}	4.52×10^{-15}
276	1.43×10^{-22}	2.36×10^{-33}	1.43×10^{-22}	7.84×10^{-16}	2.48×10^{-32}	7.84×10^{-16}	6.64×10^{-15}	8.92×10^{-30}	6.64×10^{-15}
280	2.18×10^{-22}	5.01×10^{-33}	2.18×10^{-22}	9.19×10^{-16}	4.91×10^{-32}	9.19×10^{-16}	7.32×10^{-15}	1.53×10^{-29}	7.32×10^{-15}
290	5.94×10^{-22}	3.00×10^{-32}	5.94×10^{-22}	1.34×10^{-15}	2.50×10^{-31}	1.34×10^{-15}	9.23×10^{-15}	5.49×10^{-29}	9.23×10^{-15}
295	9.58×10^{-22}	7.03×10^{-32}	9.58×10^{-22}	1.61×10^{-15}	5.41×10^{-31}	1.61×10^{-15}	1.03×10^{-14}	1.01×10^{-28}	1.03×10^{-14}
297	1.16×10^{-21}	9.81×10^{-32}	1.16×10^{-21}	1.73×10^{-15}	7.31×10^{-31}	1.73×10^{-15}	1.08×10^{-14}	1.28×10^{-28}	1.08×10^{-14}
298	1.27×10^{-21}	1.16×10^{-31}	1.27×10^{-21}	1.79×10^{-15}	8.49×10^{-31}	1.79×10^{-15}	1.10×10^{-14}	1.44×10^{-28}	1.10×10^{-14}
308	3.10×10^{-21}	5.66×10^{-31}	3.10×10^{-21}	2.52×10^{-15}	3.59×10^{-30}	2.52×10^{-15}	1.36×10^{-14}	4.47×10^{-28}	1.36×10^{-14}
328	1.59×10^{-20}	1.02×10^{-29}	1.59×10^{-20}	4.72×10^{-15}	4.95×10^{-29}	4.72×10^{-15}	2.01×10^{-14}	3.54×10^{-27}	2.01×10^{-14}
348	6.80×10^{-20}	1.32×10^{-28}	6.80×10^{-20}	8.31×10^{-15}	5.08×10^{-28}	8.31×10^{-15}	2.88×10^{-14}	2.22×10^{-26}	2.88×10^{-14}
368	2.51×10^{-19}	1.31×10^{-27}	2.51×10^{-19}	1.39×10^{-14}	4.07×10^{-27}	1.39×10^{-14}	3.98×10^{-14}	1.15×10^{-25}	3.98×10^{-14}

Table S8. The modified Arrhenius formulas for $k = AT^{B}\exp(-C/T)$ for H-abstraction and X-addition pathways.

pathways	[a]A	B	[b]C
F-R_{abs-F}	1.74×10^{-16}	1.63	256
F-R_{add-F}	2.89×10^{-22}	3.69	2457
F-R_{abs-Cl}	1.17×10^{-15}	1.41	–40
F-R_{add-Cl}	1.05×10^{-33}	7.61	1804
F-R_{abs-Br}	4.60×10^{-15}	1.31	–6
F-R_{add-Br}	9.41×10^{-107}	32.02	–6079
Cl-R_{abs-F}	1.55×10^{-19}	3.08	2415
Cl-R_{add-F}	3.27×10^{-28}	4.95	6056
Cl-R_{abs-Cl}	1.97×10^{-19}	2.74	140
Cl-R_{add-Cl}	2.11×10^{-23}	2.07	9015
Cl-R_{abs-Br}	3.70×10^{-19}	2.54	–182
Cl-R_{add-Br}	1.97×10^{-17}	1.62	6773
Br-R_{abs-F}	1.09×10^{-19}	3.44	7165
Br-R_{add-F}	4.68×10^{-15}	1.59	14095
Br-R_{abs-Cl}	7.94×10^{-19}	2.72	2309
Br-R_{add-Cl}	1.36×10^{-15}	1.40	12811
Br-R_{abs-Br}	8.33×10^{-20}	2.73	1113
Br-R_{add-Br}	6.06×10^{-18}	1.57	9948

[a] Units in cm^3 $molecule^{-1}$ s^{-1}. [b] $C = \frac{E}{R}$, $E = E_a - nRT$, in which C (in K), E (in kcal/mol) and n are the fitting parameters, and E_a (in kcal/mol) and R (in kcal/mol·K) are the activation energy and the gas constant, respectively (Zheng et al., 2010).

Table S9. The potential barrier heights (ΔE) and reaction enthalpies (ΔH^0_{298}) for elimination pathways of the F + ClCHO reaction. (in kcal/mol, the energy of the corresponding IM is set to be zero as reference)

	ΔE	ΔH^0_{298}
$F\text{-}R_{elm\text{-}Cl1}$	15.88	2.93
$F\text{-}R_{elm\text{-}Cl2}$	1.12	–13.07
$F\text{-}R_{elm\text{-}Cl3}$	32.40	–19.73

REFERENCES

Bednarek, G., Breil, M., Hoffmann, A., Kohlmann, J. P., Mors, V., and Zellner, R.: Rate and mechanism of the atmospheric degradation of 1,1,1,2-tetrafluoroethane (HFC-134a), Ber. Bunsen. Phys. Chem., 100, 528-539, 1996.

Behr, P., Goldbach, K., and Heydtmann, H.: The reaction of fuorine atoms with formyl fluoride and the CFO self-reaction at 293 K, Int. J. Chem. Kinet. , 25, 957-967, 1993.

Behr, P., Kaupert, C., Shafranovski, E., and Heydtmann, H.: Temperature dependence of the gas-phase reactions F+CHFO, CFO+F, and CFO+CFO, Int J Chem Kinet, 30, 329-333, 1998.

Catoire, V., Lesclaux, R., Schneider, W. F., and Wallington, T. J.: Kinetics and mechanisms of the self-reactions of CCl_3O_2 and $CHCl_2O_2$ radicals and their reactions with HO_2, J. Phys. Chem. , 100, 14356-14371, 1996.

Edney, E. O., and Driscoll, D. J.: Chlorine initiated photooxidation studies of hydrochlorofluorocarbons (HCFCs) and hydrofluorocarbons (HFCs): Results for HCFC-22 ($CHClF_2$); HFC-41 (CH3F); HCFC-124 ($CClFHCF_3$); HFC-125 (CF_3CHF_2); HFC-134a (CF_3CH_2F); HCFC-142b ($CClF_2CH_3$); and HFC-152a (CHF_2CH_3), Int. J. Chem. Kinet. , 24, 1067-1081, 1992.

Francisco, J. S., and Zhao, Y.: The reaction of atomic fluorine with formyl fluoride: An experimental and theoretical study, J. Chem. Phys. , 93, 276-286, 1990.

Gonzalez, J., Anglada, J. M., Buszek, R. J., and Francisco, J. S.: Impact of Water on the OH plus HOCl Reaction, J. Am. Chem. Soc. , 133, 3345-3353, 2011.

Groner, P., and Warren, R. D.: Approximate r(e) structures from experimental rotational constants and ab initio force fields, J. Mol. Struct. , 599, 323-335, 2001.

Hasson, A. S., Moore, C. M., and Smith, I. W. M.: The fluorine atom initiated oxidation of CF_3CFH_2 (HFC-134a) studied by FTIR spectroscopy, Int. J. Chem. Kinet. , 30, 541-554, 1998.

Huisman, P. A. G., Klebe, K. J., Mijlhoff, F. C., and Renes, G. H.: Molecular-structure of formyl fluoride in the gas-phase as determined from electron-diffraction and microwave data, J. Mol. Struct. , 57, 71-82, 1979.

Jensen, F.: A Remarkable Large Effect of Spin Contamination on Calculated Vibrational Frequencies, Chem. Phys. Lett. , 169, 519-528, 1990.

Ji, Y. M., Zhao, X. L., Liu, J. Y., Wang, Y., and Li, Z. S.: Theoretical dynamic studies on the reactions of CH3C(O)CH3-nCln (n=0-3) with the chlorine atom, J Comput Chem, 29, 809-819, 2008.

Libuda, H. G., Zabel, F., Fink, E. H., and Becker, K. H.: Formyl chloride: UV absorption cross sections and rate constants for the reactions with Cl and OH, J. Phys. Chem. , 94, 5860-5865, 1990.

Liu, Y. P., Lu, D. H., Gonzalezlafont, A., Truhlar, D. G., and Garrett, B. C.: Direct dynamics calculation of the kinetic isotope effect for an organic hydrogen-transfer reaction, including corner-cutting tunneling in 21 Dimensions, J. Am. Chem. Soc. , 115, 7806-7817, 1993.

Meagher, R. J., McIntosh, M. E., Hurley, M. D., and Wallington, T. J.: A kinetic study of the reaction of chlorine and fluorine atoms with HC(O)F at 295+/-2 K, Int J Chem Kinet, 29, 619-625, 1997.

Nagai, K., Yamada, C., Endo, Y., and Hirota, E.: Infrared diode-laser spectroscopy of FCO- the NU-1 and NU-2 bands, J. Mol. Spectrosc. , 90, 249-272, 1981.

NIST: http://webbook.nist.gov/chemistry/.

Orlando, J. J.: Temperature dependence of the rate coefficients for the reaction of chlorine atoms with chloromethanes, Int. J. Chem. Kinet. , 31, 515-524, 1999.

Pacey, P. D.: Changing Conceptions of Activation-Energy, J. Chem. Educ. , 58, 612-614, 1981.

Sanhueza, E., and Heicklen, J.: Chlorine-atom sensitized oxidation of dichloromethane and chloromethane, J. Phys. Chem. , 79, 7-11, 1975.

Szabo, A., and Ostlund, N. S.: Modern quantum chemistry, McGraw-Hill: New York, 1997.

Truhlar, D. G., and Garrett, B. C.: Variational Transition-State Theory, Acc. Chem. Res. , 13, 440-448, 1980.

Wallington, T. J., Hurley, M. D., Ball, J. C., and Kaiser, E. W.: Atmospheric chemistry of hydrofluorocarbon 134a: Fate of the alkoxy radical CF_3CFHO, Environ. Sci. Technol., 26, 1318-1324, 1992.

Wallington, T. J., Hurley, M. D., and Schneider, W. F.: Atmospheric chemistry of CH_3Cl: Mechanistic study of the reaction of CH_2ClO_2 radicals with HO_2, Chem. Phys. Lett. , 251, 164-173, 1996.

Wu, H. Y., Liu, J. Y., Li, Z. S., Huang, X. R., and Sun, C. C.: Theoretical study and rate constant calculation for the F+CHFO reaction, Chemical Physics Letters, 369, 504-512, 2003.

Zheng, J. J., and Truhlar, D. G.: Kinetics of hydrogen-transfer isomerizations of butoxyl radicals, Phys. Chem. Chem. Phys. , 12, 7782-7793, 2010.